Original Article

Evaluation of biocompatible alginate- and deferoxamine-coated ternary composites for magnetic resonance imaging and gene delivery into glioblastoma cells

Ken Cham-Fai Leung[1], Kathy W. Y. Sham[2], Chun-Pong Chak[3], Josie M. Y. Lai[2], Siu-Fung Lee[1,3], Yì-Xiáng J. Wáng[4], Christopher H. K. Cheng[2]

[1]Department of Chemistry, Institute of Creativity and Partner State Key Laboratory of Environmental and Biological Analysis, The Hong Kong Baptist University, Hong Kong SAR, China; [2]School of Biomedical Sciences and Center of Novel Functional Molecules, [3]Department of Chemistry, The Chinese University of Hong Kong, Shatin, Hong Kong SAR, China; [4]Department of Imaging and Interventional Radiology, Prince of Wales Hospital, The Chinese University of Hong Kong, Shatin, Hong Kong SAR, China

Correspondence to: Ken Cham-Fai Leung. Department of Chemistry, Institute of Creativity and Partner State Key Laboratory of Environmental and Biological Analysis, The Hong Kong Baptist University, Kowloon Tong, Kowloon, Hong Kong SAR, China. Email: cfleung@hkbu.edu.hk; Yì-Xiáng J. Wáng. Department of Imaging and Interventional Radiology, Prince of Wales Hospital, The Chinese University of Hong Kong, Shatin, NT, Hong Kong SAR, China. Email: yixiang_wang@cuhk.edu.hk; Christopher H. K. Cheng. School of Biomedical Sciences, The Chinese University of Hong Kong, Shatin, NT, Hong Kong SAR, China. Email: chkcheng@cuhk.edu.hk.

Background: This paper describes comparative studies in cytotoxicities, magnetic resonance imaging (MRI), and gene delivery into glioblastoma U87MG or U138MG cells with ternary composites that are consist of superparamagnetic iron oxide (SPIO) nanoparticles (NPs) (size: 8-10 nm) with different surface coatings, circular plasmid DNA (pDNA) (~4 kb) equipped with fluorescent/luminescent probe, and branched polyethylenimine (25 kDa, PDI 2.5).

Methods: Three types of SPIO-NPs were used, including: (I) naked iron oxide NPs with Fe-OH surface group (Bare-NP); (II) iron oxide NPs with a coating of alginate (Alg-NPs); and (III) iron oxide NPs with a coating of deferoxamine (Def-NPs). By tuning the polyethylenimine (PEI)/NP ratios and with a fixed DNA amount, different ternary composites were employed for NP/gene transfection into glioblastoma U87MG or U138MG cells, which were then characterized by Prussian blue staining, *in vitro* MRI, green fluorescence protein (GFP) fluorescence and luciferase assay.

Results: Among the composites prepared, 0.2 ng PEI/0.5 μg DNA/1.0 μg Bare-NP ternary composite possessed the best cellular uptake efficiency of NP to the cytoplasm, following the trend Bare-NP > Alg-NP > Def-NP. This observation was consistent to the MRI assessments with *in vitro* T_2 relaxivity (r_2) values of 46.0, 35.5, and 23.7 $s^{-1}\cdot\mu M^{-1}\cdot$Fe, respectively. For cellular uptake efficiency of the pDNA, all variations of PEI/NP ratios of the composites did not yield significant differences. However, cellular uptake efficiencies of pDNA in the ternary composites in U138MG cells were generally higher than that of U87MG cells by an order of magnitude. Exceptionally, the ternary composite 0.2 ng PEI/0.5 μg DNA/1.0 μg Bare-NP possessed a lowered luciferase activity RLU for gene expression in U138MG cells. A total of 0.2 ng PEI/0.5 μg DNA/0.1 μg Bare-NP would be uptaken to the cell nucleus with the highest luciferase activity. A working concentration range of PEI with at least 15% higher cell viabilities than lipofectamine was 0.1 to 0.2 ng/well. The cytotoxicities became significant when 0.5 ng/well PEI was present in the ternary composites.

Conclusions: The as-prepared composites offer potential biomedical applications in simultaneous gene delivery, imaging contrast enhancement, and metabolism study.

Keywords: Deferoxamine (Def); gene delivery; imaging agents; nanoparticles (NPs); organic-inorganic hybrid composites

Submitted Mar 03, 2015. Accepted for publication Mar 10, 2015.
doi: 10.3978/j.issn.2223-4292.2015.03.12
View this article at: http://dx.doi.org/10.3978/j.issn.2223-4292.2015.03.12

Introduction

The development of diagnostic and therapeutic nanomaterials (1-8) for drug/gene co-delivery and ultrasonic/magnetic resonance imaging (MRI) contrast enhancement has been progressing rapidly towards various cancer cell types (9-25). In particular, superparamagnetic iron oxide (SPIO) nanoparticles (NPs) can offer imaging cell tracking, magnetic targeting, and substrate delivery to specific target site(s) (26-28). Linear polyethylenimine (PEI) polymers of low or high molecular weights have been employed to deliver genes with enhanced transfection efficiencies and possibly reducing cytotoxicities (29-39). However, branched PEI has been less studied. SPIO-NPs that are coated with alginate (Alg) polymer derivatives, may show enhanced biocompatibility and colloidal stability (40-42). In particular, ultrasmall deferoxamine (Def)-coated SPIO-NPs were first reported in our group (9,15) and studied for their biomedical properties. Def, also known as desferal, is a clinically approved drug to treat iron poisoning. Slow degradation of iron oxide NPs *in vivo* will result in soluble iron ions which will, in turn, capture by Def layer at the NPs' periphery. Eventually, the Def-iron complexes will be excreted in the urine, thus reducing the *in vivo* toxicity especially for the heart and liver.

In view of delivering genes and facilitating MRI towards glioblastoma U87MG cells with enhanced cellular uptake or transfection efficiencies, we report herein the use of bare-, Alg-coated, and Def-coated ultrasmall (8-10 nm) Fe_3O_4 SPIO-NPs, hybridizing individually with circular plasmid DNAs (pDNA) (pEGFP-C1 and pRL-CMV), and branched PEI (25 kDa, PDI =2.5) to furnish ternary composites (9,15,16,32,43) for MRI, fluorescence imaging, and cytotoxicity evaluation. Different coatings on the SPIO-NPs (Bare-NP, Alg-NP, and Def-NP) have been shown to demonstrate different effects toward the cellular uptake (16,44,45) into brain tumor cells. Circular pDNA pEGFP-C1 (~4.7 kb) was encoded with a red-shifted variant of wild-type green fluorescence protein (GFP) in mammalian cells whereas circular pDNA pRL-CMV (~4.0 kb) was encoded with *Renilla* luciferase in various cell types. As markers, the fluorescence or luminescence intensity is directly proportional to the amount of GFP/RLU. By the strong, enhanced and constitutive expression of the reporters, the signals can be easily detected. They were optimized so that the reporters can be expressed in a variety of cell types/lines. By using two signal detection methods, any reduction or enhancement of DNA uptake by the composites can be estimated by different aspects. It is envisaged that after the cellular uptake of the composites into the cells, the NPs in the composites would be cleaved and localized in the cytoplasm, which is responsible for generating MRI dark contrast signal. On the other hand, the pDNA of the composites will be further imported into the nucleus, which is responsible for expressing the fluorescence/luminescence.

Materials and methods

Synthesis

Ultrasmall SPIO-NP with average diameter of 8-10 nm (Bare-NPs) was synthesized according to literature procedures (26-28). Alg-NPs and Def-NPs were synthesized according to literature procedures (9,15,16). For the synthesis of composites, a stock solution of branched PEI was prepared with a concentration of 10 ng/μL in water. By serial dilutions, the solutions of branched PEI with different concentrations were added to the culture medium (250 μL) containing the DNA. After incubation for 30 min, pre-ultrasonicated, bare-, Alg-, or Def-NPs of known particle and iron concentrations in water were added to the mixture, gently mixed and incubated for further 30 min to obtain the composites.

Plasmid DNA

All circular pDNAs for transfection were prepared using the QIAprep Spin Miniprep Kit (QIAGEN, Hilden, Germany) with A260/A280 ratio larger than 1.8. Plasmid pEGFP-C1 (~4.7 kb, Clontech, CA, USA) encodes a reporter comprising a red-shifted variant of wild-type GFP for expression in mammalian cells. The green fluorescence of the transfected U87MG or U138MG cells was visualized by a Nikon TE2000 fluorescence microscope 24 h after the transfection. Plasmid pRL-CMV (~4.0 kb, Promega) encodes a reporter comprising *Renilla* luciferase for expression in various cell types. Luminescence was detected by a luminometer (GloMax 20/20 Luminometer, Promega) 24 h after the transfection of U87MG or U138MG cells. The luciferase activity (RLU) was normalized against total cellular protein per well and expressed as RLU/μg protein.

Cell culture

U87MG and U138MG cells were obtained from American Type Culture Collection (ATCC, Manassas, VA, USA). Cells were cultured with α-MEM (Life Technologies)

containing 10% fetal bovine serum (FBS), 100 U/mL penicillin, and 100 μg/mL streptomycin at 37 ℃ and in a humidified 5% CO_2 atmosphere.

Cellular uptake

About 5,000 cells were seeded onto each well of the 96-well plates for methylthiazolyldiphenyl-tetrazolium bromide (MTT) assay while about 50,000 cells were seeded onto each well of the 24-well plates for luciferase and GFP observation. Next day (day 2), the culture medium was replaced with the serum-free DMEM containing different composites. After incubation for 5 h, the medium was aspirated and refreshed with complete α-MEM. The cells were incubated for further 24 h at 37 ℃ (N=2) for subsequent end-point measurements (day 3).

Prussian blue staining

After the cell transfection of the composites, U87MG cells were washed with PBS to remove any free composites. Cells were then fixed using paraformaldehyde (4%) for 40 min. Subsequently, cells were washed with PBS and incubated with freshly prepared Perls' reagent (4% potassium ferrocyanide/12% HCl, 1:1 v/v) for 30 min. Cells were washed with PBS (3×), counterstained with neutral red (0.02%), and subsequently observed by an inverted bright-field optical microscope (Nikon TE2000).

Intracellular iron content measurement

Colorimetric method was used to study the iron concentration for the cells that were transfected with the composites. After incubation of the composites for 5 h on day 2, the cells were washed, collected, and counted for the intracellular iron content quantification on day 3. After centrifugation (4,500 g) for 5 min, the collected cell pellets were dispensed in 100 μL 12% HCl solution and incubated at 60 ℃ for 4 h. After incubation, the suspension was centrifuged (12,000 g) for 10 min, whereas the supernatants were collected for iron concentration quantification. A sample solution (50 μL) was added into the wells of a 96-well plate, and then ammonium persulfate (50 μL, 1%) was added to oxidize the ferrous ions into ferric ions. Finally, potassium thiocyanate (100 μL, 0.1 M) was added to the solution and incubated for 5 min to form the red color of iron-thiocyanate. The absorption at 490 nm of the sample was observed on a microplate reader (Bio-Rad, Model 3550).

Biocompatibility assay

The cytotoxicities of cells incubated with different composites were examined by MTT assay in U87MG cells. A total of 5,000 cells were seeded onto the wells of a 96-well plate. On day 3, 10 μL of 5 mg/mL MTT was added into each well. After incubation for 3 h, the medium was removed, and formazan crystals were dissolved in dimethyl sulfoxide (150 μL) for 10 min on a shaker. A circular disc-like magnet was placed under the plate to attract the magnetic composite-uptaken cells to the bottom of the well. After that, 100 μL of the supernatant was transferred to another 96-well plate. Absorbance of each well was measured on a microplate reader (Bio-Rad, Model 3550) at a wavelength of 540 nm. The relative cell viability (%) for each sample which is related to control well, was calculated.

In vitro MRI

In vitro MRI was performed with U87MG cells 24 h after transfection. After washing with PBS, the cells were trypsinized and counted. Different numbers (12.5k, 25k, 50k, 100k, 150k, and 300k) of cells were placed in an Eppendorf tube (1.5 mL) separately. After a centrifugation at 3,000 ×g for 5 min, the Eppendorf tubes were placed perpendicular to the main magnetic induction field ($B0$) in a 20 cm × 12 cm × 8 cm water bath. MRI was performed with a 3.0-T clinical whole-body magnetic resonance unit (Achieva, Philips Medical Systems, Netherlands), using a transmit-receive head coil. The magnetic resonance sequence was a two-dimensional gradient-echo sequence with TR/TE =400/48 ms, flip angle =18°, matrix =512×256, resolution =0.45 mm × 0.45 mm, slice thickness =2 mm, and number of excitations =2. Sagittal images were obtained through the central section of the bottom tips of the Eppendorf tubes. The areas of signal void at the bottom of the Eppendorf tubes due to U87MG cells transfected with NP-containing composites from which the NPs is MRI-responsive contrast agent. T_2 relaxation times were measured by using a standard Carr-Purcell-Meiboom-Gill pulse sequence [repetition time (TR) =2,000 ms, echo time (TE) range =30-960 ms, 32 echoes, field-of-view (FOV) =134×67 mm^2, matrix =128×64, slice thickness =5 mm, number of excitations =3]. T_2 relaxation times were calculated by fitting the logarithmic region of interest signal amplitudes versus TE. The T_2 relaxivities (r_2) were determined by a linear fit of the inverse relaxation times as a function of the iron concentrations used.

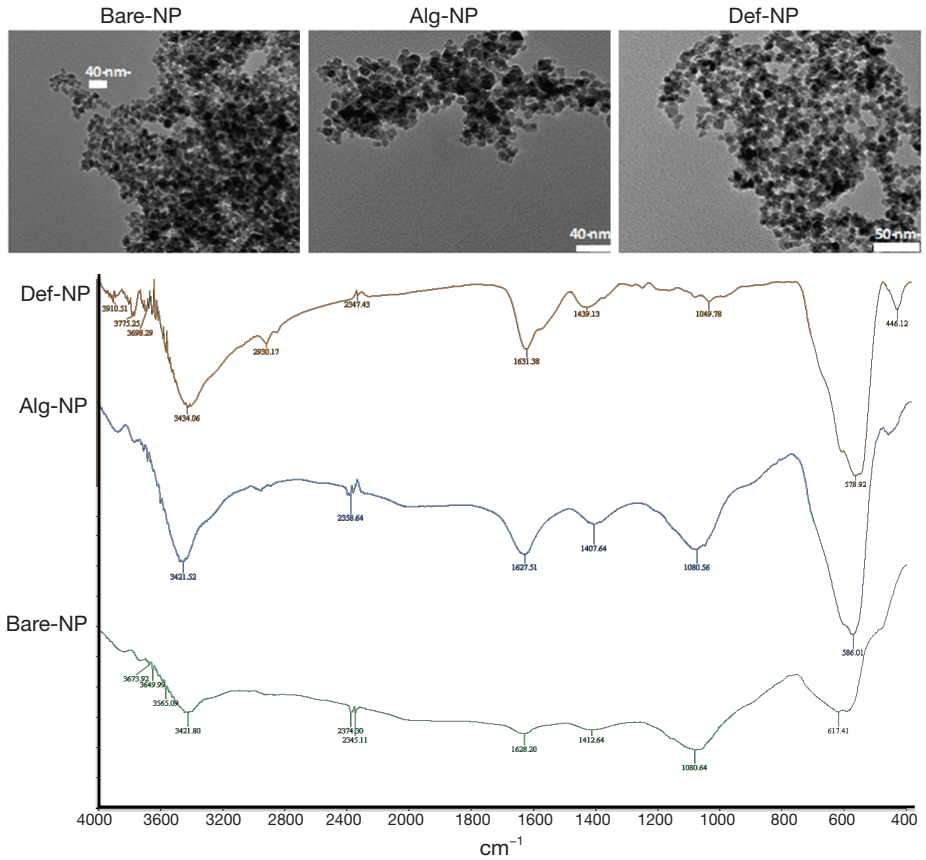

Figure 1 TEM images (A) and FTIR spectra (B) of different functionalized SPIO-NPs. Bare-NP, SPIO-NP without coating; Alg-NP, SPIO-NP with alginate coating; Def-NP, SPIO-NP with deferoxamine coating. SPIO-NPs, superparamagnetic iron oxide nanoparticles; TEM, transmission electron microscopy.

Results and discussion

NPs with different coatings, hydroxyl (Bare-NP), Alg-NP, and Def-NP, could be self-assembled with negatively charged pDNA and positively charged branched PEI to furnish ternary composites (200-300 nm) (9,15,16) thereby stabilizing by multiple electrostatic interaction and hydrogen bonds (46). The morphology and surface functional groups of the composites were characterized (*Figure 1*) by transmission electron microscopy (TEM) and infrared (IR) absorption spectroscopy, respectively, which have been reported in the literature. The as-prepared Bare-NP, Alg-NP, and Def-NP have narrow size distributions (8-10 nm). IR spectra of these NPs reveal their functional group characteristics. Bare-NP reveals IR signals (cm^{-1}) at 617 (Fe-O stretching), 1,081 (C-OH stretching), and 3,421 (O-H stretching). Alg-NP reveals IR signals (cm^{-1}) at 586 (Fe-O stretching), 1,081 (C-OH stretching), 1,407 (carboxylate), 1,628 (carboxylate carbonyl), and 3,422 (O-H stretching). Def-NP reveals IR signals (cm^{-1}) at 578 (Fe-O stretching), 1,049 (C-OH stretching), 1,631 (amide carbonyl), and 3,434 (O-H and N-H stretching).

For each NP with different coatings, hydroxyl (Bare-NP), Alg-NP, and Def-NP, six composites were prepared with varying the amount of NPs (0.1 and 1.0 μg/well), together with fixed amounts of PEI (0.2 ng/well) and pDNA (0.5 μg/well). The typical Prussian blue staining images of U87MG cells which have been separately internalized with the six composites, are shown in *Figure 2*. According to the visual assessment of these six images with blueness, based on the stained SPIO-NPs, the cellular uptake efficiencies generally increase as NP concentration increased from 0.1 to 1.0 μg/well for all cases of using Bare-NP, Alg-NP, and Def-NP. Comparatively, among these six composites, 0.2 ng PEI/0.5 μg DNA/1.0 μg Bare-NP composite possessed the best cellular uptake efficiency of NP to the

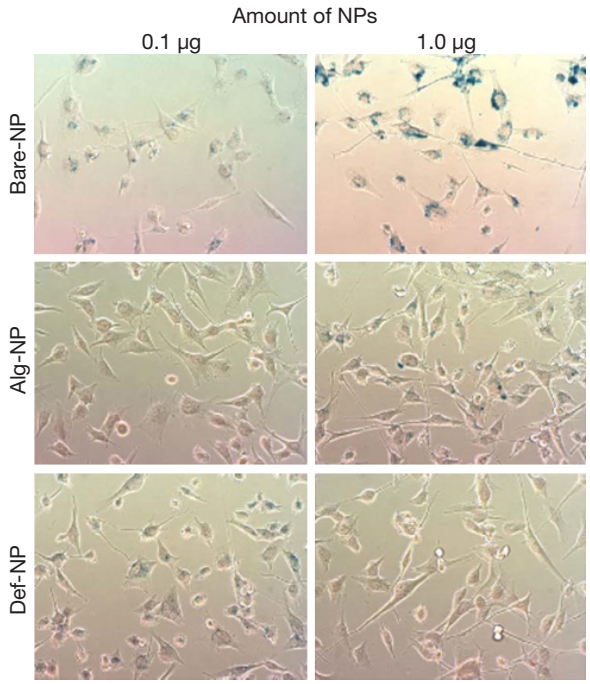

Figure 2 Prussian staining images of different composites with varying amounts of Bare-NP, Alg-NP, and Def-NP 24 h after transfection in U87MG cells. The PEI and pDNA (pEGFP-C1) concentrations of all complexes were fixed at 0.2 ng and 0.5 μg/well, respectively. Bare-NP, SPIO-NP without coating; Alg-NP, SPIO-NP with alginate coating; Def-NP, SPIO-NP with deferoxamine coating. SPIO-NPs, superparamagnetic iron oxide nanoparticles; PEI, polyethylenimine; pDNA, plasmid DNA.

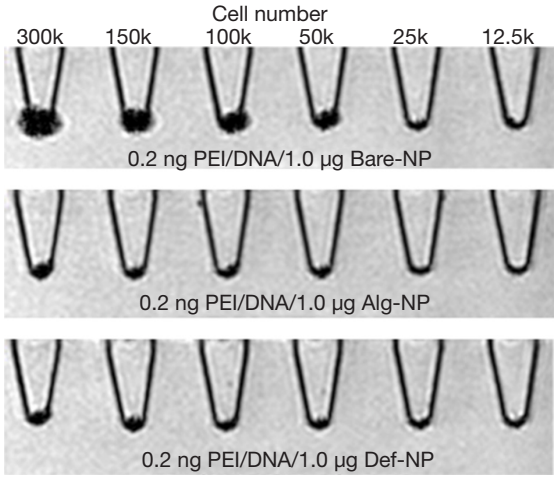

Figure 3 Gradient echo *in vitro* MRI images of composite-transfected U87MG cells in Eppendorf tubes with culture medium. The amount of pDNA (pEGFP-C1) of all complexes was fixed at 0.5 μg/well. Bare-NP, SPIO-NP without coating; Alg-NP, SPIO-NP with alginate coating; Def-NP, SPIO-NP with deferoxamine coating. SPIO-NP, superparamagnetic iron oxide nanoparticle; PEI, polyethylenimine; MRI, magnetic resonance imaging; pDNA, plasmid DNA.

cytoplasm of U87MG cells while that of other two types of NPs were similar.

U87MG cells that were transfected separately with three different composites by using three different NP coatings with fixed PEI (0.2 ng/well), DNA (0.5 μg/well), and NP (1.0 μg/well) amounts, were analyzed by *in vitro* MRI. Substantial dark contrast MRI signals with "ballooning" effect were observed as shown *Figure 3* with the cells that were centrifugated at the bottom of Eppendorf tube. Increasing number of composite-transfected cells gave a stronger MRI dark contrast signal. For all three cases separately present with Bare-NP, Alg-NP, and Def-NP, the dark MRI contrast signals with a cell number of 12.5k were still observable. The *in vitro* T_2 relaxivities (r_2) of the composites that contained Bare-NP, Alg-NP, and Def-NP were determined to be 46.0, 35.5, and 23.7 $s^{-1}\cdot\mu M^{-1}\cdot$Fe, respectively. Comparatively, the composites with Bare-NPs possessed the highest MRI signal intensities than Alg-NPs and than Def-NPs. These results were consistent to the cell uptake efficiencies determined by Prussian blue staining (*Figure 2*). Comparatively, the MRI detection was more sensitive than Prussian blue staining.

The typical GFP green fluorescent images of U87MG cells which had been separately internalized with twelve different composites of different amounts of PEI (0.1 and 0.2 ng/well) and NPs (0.1 and 1.0 μg/well) are shown in *Figure 4*. According to the visual assessment of these images, somewhat interestingly, the gene delivery efficiencies generally decreased with increasing NP amount from 0.1 to 1.0 μg/well. On the other hand, the cellular uptake efficiencies of the pDNA with different PEI amounts were generally higher with 0.1 ng/well for the cases of Alg-NP and Def-NP. For Bare-NP, the fluorescent intensities using PEI of 0.1 or 0.2 ng/well were similar. Comparatively, 0.1 ng PEI/0.5 μg DNA/0.1 μg Alg-NP and 0.1 ng PEI/0.5 μg DNA/0.1 μg Def-NP composites possessed the highest cellular uptake efficiency of the pDNA to the cell nucleus among others. It is reasonably to consider that the cellular uptake efficiency depends on the surface charge density, stability of the composites and further cleavage of the composite with NP localized in cytoplasm and pDNA in

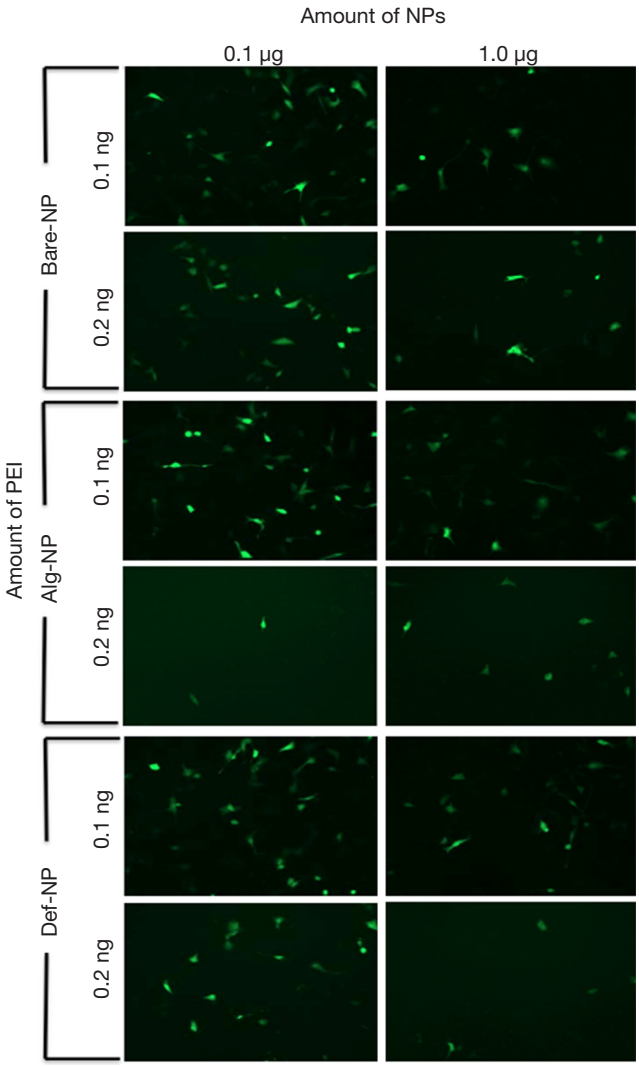

Figure 4 GFP fluorescence images of different composites with varying amounts of Bare-NP, Alg-NP, and Def-NP (0.1 and 1.0 μg) as well as PEI (0.1 and 0.2 ng) 24 h after transfection in U87MG cells. The DNA pEGFP-C1 concentration of all complexes was fixed at 0.5 μg/well. Bare-NP, SPIO-NP without coating; Alg-NP, SPIO-NP with alginate coating; Def-NP, SPIO-NP with deferoxamine coating. SPIO-NP, superparamagnetic iron oxide nanoparticle; GFP, green fluorescence protein; PEI, polyethylenimine.

nucleus. The transfected composites would eventually be dissociated into separate components and subject to an efflux mechanism. Therefore, it is essential to tune the components' ratios to understand the efficiencies in transfecting NP and gene towards glioblastoma cells.

Plasmid DNA pRL-CMV carries a *Renilia* luciferase gene thus it has to be translocated into the nucleus of the cells for gene transcription process. The amount of DNA that was successfully transfected, is directly proportional to the luminescent signal generated from luciferase expression. Therefore, a high luciferase activity with the composites reveals higher gene delivery efficiency into the cells. Luciferase expression of U87MG cells that were transfected with the pRL-CMV-containing composites, revealed approximately a luminescent in a range of 10^4 to 10^5 RLU (*Figure 5*). Most of the composites had a RLU value higher than that of the commercially available transfecting agent lipofectamine which was a positive control in the present study. On the other hand, the luciferase expression of U138MG cells transfected with the pRL-CMV-containing composites revealed an increased luminescent in a range of 10^5 to 10^6 RLU (*Figure 6*). Noticeably, the gene expression of the composite 0.2 ng PEI/0.5 μg DNA/1.0 μg Bare-NP towards U138MG cells was exceptionally low as revealed in the luminescence approximately of 10^3 RLU. However, 0.2 ng PEI/0.5 μg DNA/0.1 μg Bare-NP gave the highest luciferase activity in both cell lines.

Eighteen ternary composites were prepared and their cytotoxicities in U87MG cells were evaluated by MTT assay and compared with several controls-medium, lipofectamine, PEI alone, and PEI/DNA (*Figure 7*). Generally, percentage cell viabilities decreased with increasing amounts of PEI from 0.1 ng/well or 0.2 ng/well (75-90%) to 0.5 ng/well (30-50%). These results revealed that the cytotoxicity of using 0.5 ng PEI was higher than lipofectamine. Furthermore, the best working PEI concentration range was between 0.1 and 0.2 ng/well in our experiment.

Conclusions

Different ternary composites based on PEI/DNA/Bare-NP, Alg-NP, or Def-NP have been prepared by tuning the PEI/NP ratios and with a fixed DNA amount, for transfection into glioblastoma U87MG or U138MG cells. The transfection efficiencies involving NP uptake and gene expression with the ternary composites could be altered by tuning the PEI/NP ratios in the composite, which were characterized by Prussian blue staining, *in vitro* MRI, GFP fluorescence, and luciferase expression. Among the composites prepared, 0.2 ng PEI/0.5 μg DNA/1.0 μg Bare-NP ternary composite possessed the best cellular uptake efficiency of NP to the cytoplasm, following the trend Bare-NP > Alg-NP > Def-NP. This observation was consistent to the MRI assessments with *in vitro* T_2

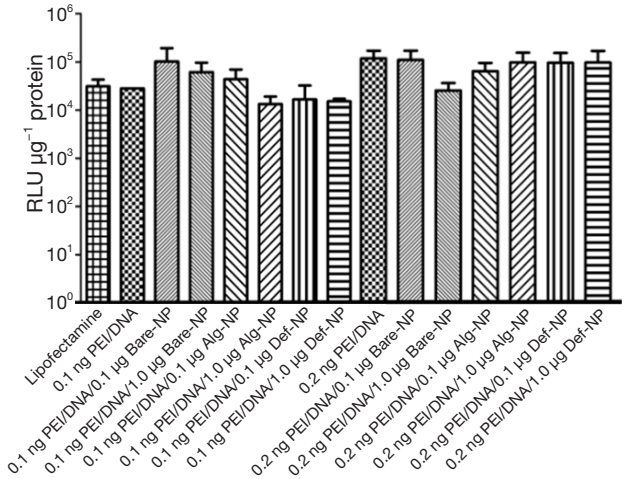

Figure 5 Luciferase expression in composite-transfected U87MG cells. The amount of pDNA (pRL-CMV) of all complexes was fixed at 0.5 μg/well. Bare-NP, SPIO-NP without coating; Alg-NP, SPIO-NP with alginate coating; Def-NP, SPIO-NP with deferoxamine coating. SPIO-NP, superparamagnetic iron oxide nanoparticle; RLU, luciferase activity; PEI, polyethylenimine; pDNA, plasmid DNA.

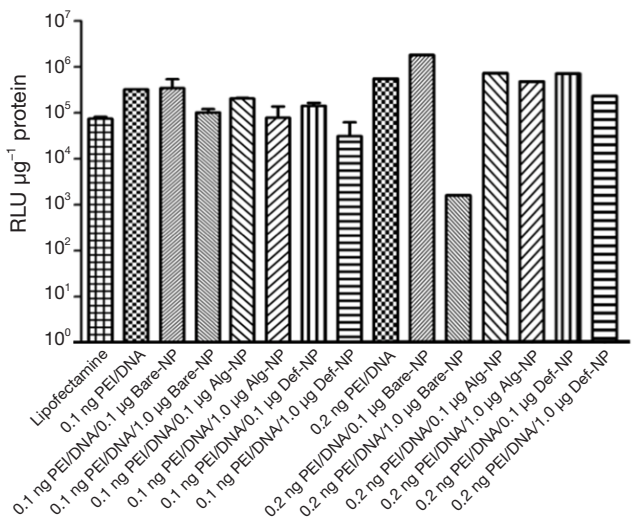

Figure 6 Luciferase expression in composite-transfected U138MG cells. The amount of pDNA (pRL-CMV) of all complexes was fixed at 0.5 μg/well. Bare-NP, SPIO-NP without coating; Alg-NP, SPIO-NP with alginate coating; Def-NP, SPIO-NP with deferoxamine coating. SPIO-NP, superparamagnetic iron oxide nanoparticle; RLU, luciferase activity; PEI, polyethylenimine; pDNA, plasmid DNA.

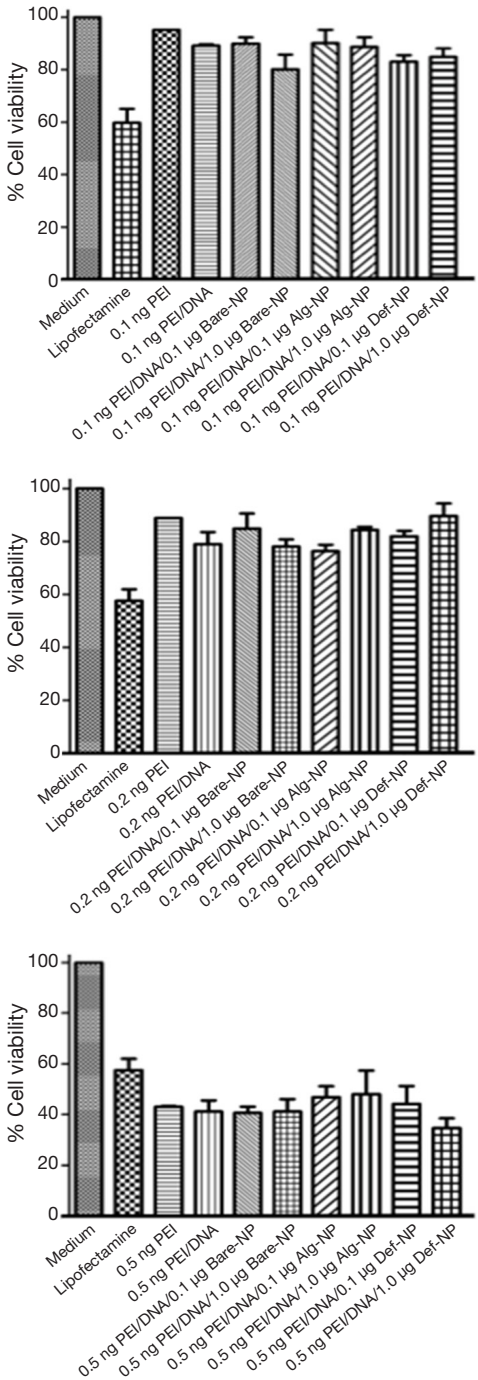

Figure 7 Cell viability of U87MG cells as determined by MTT assay 24 h after incubation with each composite for 5 h. The amount of pDNA (pEGFP-C1) of all composites was fixed at 0.5 μg/well. Bare-NP, SPIO-NP without coating; Alg-NP, SPIO-NP with alginate coating; Def-NP, SPIO-NP with deferoxamine coating. SPIO-NP, superparamagnetic iron oxide nanoparticle; PEI, polyethylenimine; pDNA, plasmid DNA.

relaxivity (r_2) values of 46.0, 35.5, and 23.7 $s^{-1}\cdot\mu M^{-1}\cdot$Fe, respectively. For cellular uptake efficiency of the pDNA, all variations of PEI/NP ratios of the composites did not possess significant differences. However, cellular uptake efficiencies of pDNA in the ternary composites in U138MG cells were generally higher than that of U87MG cells by an order of magnitude. Exceptionally, the ternary composite 0.2 ng PEI/0.5 μg DNA/1.0 μg Bare-NP possessed a lowered luciferase activity in U138MG cells. A total of 0.2 ng PEI/0.5 μg DNA/0.1 μg Bare-NP would be uptaken to the cell nucleus with the highest luciferase activity. A working concentration range of PEI with at least 15% higher cell viabilities than lipofectamine is 0.1 to 0.2 ng/well. The cytotoxicities become significant when 0.5 ng/well PEI is present in the ternary composites. As a result, as-prepared composites or other novel nanostructured magnetic composites (47,48) offer potential biomedical applications in simultaneous gene delivery, imaging contrast enhancement, and metabolism study for the next generation *in vivo* carcinoma nano-theranostic purpose.

Acknowledgements

We acknowledge the financial support by HKRGC-GRF [201213] and AoE/P-03/08 research grants.

Disclosure: The authors declare no conflicts of interest.

References

1. Moyano DF, Rotello VM. Nano meets biology: structure and function at the nanoparticle interface. Langmuir 2011;27:10376-85.
2. Ambrogio MW, Thomas CR, Zhao YL, Zink JI, Stoddart JF. Mechanized silica nanoparticles: a new frontier in theranostic nanomedicine. Acc Chem Res 2011;44:903-13.
3. Zhang Q, Liu F, Nguyen KT, Ma X, Wang X, Xing B, Zhao Y. Multifunctional mesoporous silica nanoparticles for cancer-targeted and controlled drug delivery. Adv Funct Mater 2012;22:5144-56.
4. Yan H, Teh C, Sreejith S, Zhu L, Kwok A, Fang W, Ma X, Nguyen KT, Korzh V, Zhao Y. Functional mesoporous silica nanoparticles for photothermal-controlled drug delivery in vivo. Angew Chem Int Ed Engl 2012;51:8373-7.
5. Kelkar SS, Reineke TM. Theranostics: combining imaging and therapy. Bioconjug Chem 2011;22:1879-903.
6. Algar WR, Prasuhn DE, Stewart MH, Jennings TL, Blanco-Canosa JB, Dawson PE, Medintz IL. The controlled display of biomolecules on nanoparticles: a challenge suited to bioorthogonal chemistry. Bioconjug Chem 2011;22:825-58.
7. Smith BA, Smith BD. Biomarkers and molecular probes for cell death imaging and targeted therapeutics. Bioconjug Chem 2012;23:1989-2006.
8. Xuan S, Wang F, Gong X, Kong SK, Yu JC, Leung KC. Hierarchical core/shell Fe3O4@SiO2@γ-AlOOH@Au micro/nanoflowers for protein immobilization. Chem Commun (Camb) 2011;47:2514-6.
9. Leung KC, Chak CP, Lee SF, Lai JM, Zhu XM, Wang YX, Sham KW, Cheng CH. Enhanced cellular uptake and gene delivery of glioblastoma with deferoxamine-coated nanoparticle/plasmid DNA/branched polyethylenimine composites. Chem Commun (Camb) 2013;49:549-51.
10. Nair M, Guduru R, Liang P, Hong J, Sagar V, Khizroev S. Externally controlled on-demand release of anti-HIV drug using magneto-electric nanoparticles as carriers. Nat Commun 2013;4:1707.
11. Wohlfart S, Gelperina S, Kreuter J. Transport of drugs across the blood-brain barrier by nanoparticles. J Control Release 2012;161:264-73.
12. Koffie RM, Farrar CT, Saidi LJ, William CM, Hyman BT, Spires-Jones TL. Nanoparticles enhance brain delivery of blood-brain barrier-impermeable probes for in vivo optical and magnetic resonance imaging. Proc Natl Acad Sci U S A 2011;108:18837-42.
13. Lu J, Ma S, Sun J, Xia C, Liu C, Wang Z, Zhao X, Gao F, Gong Q, Song B, Shuai X, Ai H, Gu Z. Manganese ferrite nanoparticle micellar nanocomposites as MRI contrast agent for liver imaging. Biomaterials 2009;30:2919-28.
14. Tam KY, Leung KC, Wang YX. Chemoembolization agents for cancer treatment. Eur J Pharm Sci 2011;44:1-10.
15. Leung KC, Chak CP, Lee SF, Lai JM, Zhu XM, Wang YX, Sham KW, Wong CH, Cheng CH. Increased efficacies in magnetofection and gene delivery to hepatocellular carcinoma cells with ternary organic-inorganic hybrid nanocomposites. Chem Asian J 2013;8:1760-4.
16. Leung KC, Lee SF, Wong CH, Chak CP, Lai JM, Zhu XM, Wang YX, Sham KW, Cheng CH. Nanoparticle-DNA-polymer composites for hepatocellular carcinoma cell labeling, sensing, and magnetic resonance imaging. Methods 2013;64:315-21.
17. Chou LY, Ming K, Chan WC. Strategies for the intracellular delivery of nanoparticles. Chem Soc Rev 2011;40:233-45.

18. Xuan S, Wang F, Lai JM, Sham KW, Wang YX, Lee SF, Yu JC, Cheng CH, Leung KC. Synthesis of biocompatible, mesoporous Fe(3)O(4) nano/microspheres with large surface area for magnetic resonance imaging and therapeutic applications. ACS Appl Mater Interfaces 2011;3:237-44.
19. Leung KC, Xuan S, Zhu X, Wang D, Chak CP, Lee SF, Ho WK, Chung BC. Gold and iron oxide hybrid nanocomposite materials. Chem Soc Rev 2012;41:1911-28.
20. Zhu XM, Yuan J, Leung KC, Lee SF, Sham KW, Cheng CH, Au DW, Teng GJ, Ahuja AT, Wang YX. Hollow superparamagnetic iron oxide nanoshells as a hydrophobic anticancer drug carrier: intracelluar pH-dependent drug release and enhanced cytotoxicity. Nanoscale 2012;4:5744-54.
21. Xuan SH, Lee SF, Lau JT, Zhu X, Wang YX, Wang F, Lai JM, Sham KW, Lo PC, Yu JC, Cheng CH, Leung KC. Photocytotoxicity and magnetic relaxivity responses of dual-porous γ-Fe2O3@meso-SiO2 microspheres. ACS Appl Mater Interfaces 2012;4:2033-40.
22. Lee SF, Zhu XM, Wang YX, Xuan SH, You Q, Chan WH, Wong CH, Wang F, Yu JC, Cheng CH, Leung KC. Ultrasound, pH, and magnetically responsive crown-ether-coated core/shell nanoparticles as drug encapsulation and release systems. ACS Appl Mater Interfaces 2013;5:1566-74.
23. Wang DW, Zhu XM, Lee SF, Chan HM, Li HW, Kong SK, Yu JC, Cheng CH, Wang XY, Leung KC. Folate-conjugated Fe3O4@SiO2@gold nanorods@mesoporous SiO2 hybrid nanomaterial: a theranostic agent for magnetic resonance imaging and photothermal therapy. J Mater Chem B 2013;1:2934-42.
24. Wang YX, Wang DW, Zhu XM, Zhao F, Leung KC. Carbon coated superparamagnetic iron oxide nanoparticles for sentinel lymph nodes mapping. Quant Imaging Med Surg 2012;2:53-6.
25. Lee JH, Chen KJ, Noh SH, Garcia MA, Wang H, Lin WY, Jeong H, Kong BJ, Stout DB, Cheon J, Tseng HR. On-demand drug release system for in vivo cancer treatment through self-assembled magnetic nanoparticles. Angew Chem Int Ed Engl 2013;52:4384-8.
26. Wang HH, Wang YX, Leung KC, Au DW, Xuan S, Chak CP, Lee SK, Sheng H, Zhang G, Qin L, Griffith JF, Ahuja AT. Durable mesenchymal stem cell labelling by using polyhedral superparamagnetic iron oxide nanoparticles. Chemistry 2009;15:12417-25.
27. Wang YX, Quercy-Jouvet T, Wang HH, Li AK, Chak CP, Xuan S, Shi L, Wang DF, Lee SF, Leung PC, Lau CB, Fung KP, Leung KC. Efficacy and Durability in Direct Labeling of Mesenchymal Stem Cells Using Ultrasmall Superparamagnetic Iron Oxide Nanoparticles with Organosilica, Dextran, and PEG Coatings. Materials 2011;4:703-15.
28. Zhu XM, Wang YX, Leung KC, Lee SF, Zhao F, Wang DW, Lai JM, Wan C, Cheng CH, Ahuja AT. Enhanced cellular uptake of aminosilane-coated superparamagnetic iron oxide nanoparticles in mammalian cell lines. Int J Nanomedicine 2012;7:953-64.
29. McBain SC, Yiu HH, Haj AE, Dobson J. Polyethyleneimine functionalized iron oxide nanoparticles as agents for DNA delivery and transfection. J Mater Chem 2007;17:2561-5.
30. Steitz B, Hofmann H, Kamau SW, Hassa PO, Hottiger MO, von Rechenberg B, Hofmann-Amtenbrink M, Petri-Fink A. Characterization of PEI-coated superparamagnetic iron oxide nanoparticles for transfection: Size distribution, colloidal properties and DNA interaction. J Magn Magn Mater 2007;311:300-5.
31. Ito T, Iida-Tanaka N, Koyama Y. Efficient in vivo gene transfection by stable DNA/PEI complexes coated by hyaluronic acid. J Drug Target 2008;16:276-81.
32. Lee Y, Miyata K, Oba M, Ishii T, Fukushima S, Han M, Koyama H, Nishiyama N, Kataoka K. Charge-conversion ternary polyplex with endosome disruption moiety: a technique for efficient and safe gene delivery. Angew Chem Int Ed Engl 2008;47:5163-6.
33. Wang XL, Zhou LZ, Ma YJ, Gu HC. Charged magnetic nanoparticles for enhancing gene transfection. IEEE Trans. Nanotechnol 2009;8:142-6.
34. Xia T, Kovochich M, Liong M, Meng H, Kabehie S, George S, Zink JI, Nel AE. Polyethyleneimine coating enhances the cellular uptake of mesoporous silica nanoparticles and allows safe delivery of siRNA and DNA constructs. ACS Nano 2009;3:3273-86.
35. Yiu HH, McBain SC, Lethbridge ZA, Lees MR, Dobson J. Preparation and characterization of polyethylenimine-coated Fe3O4-MCM-48 nanocomposite particles as a novel agent for magnet-assisted transfection. J Biomed Mater Res A 2010;92:386-92.
36. Miyata K, Gouda N, Takemoto H, Oba M, Lee Y, Koyama H, Yamasaki Y, Itaka K, Nishiyama N, Kataoka K. Enhanced transfection with silica-coated polyplexes loading plasmid DNA. Biomaterials 2010;31:4764-70.
37. Cabral H, Kataoka K. Multifunctional nanoassemblies of block copolymers for future cancer therapy. Sci Technol Adv Mater 2010;11:014109.

38. Liu WM, Xue TN, Peng N, He WT, Zhuo RX, Huang SW. Dendrimer modified magnetic iron oxide nanoparticle/DNA/PEI ternary magnetoplexes: a novel strategy for magnetofection. J Mater Chem 2011;21:13306-15.
39. Vachutinsky Y, Oba M, Miyata K, Hiki S, Kano MR, Nishiyama N, Koyama H, Miyazono K, Kataoka K. Antiangiogenic gene therapy of experimental pancreatic tumor by sFlt-1 plasmid DNA carried by RGD-modified crosslinked polyplex micelles. J Control Release 2011;149:51-7.
40. Ma HL, Qi XR, Maitani Y, Nagai T. Preparation and characterization of superparamagnetic iron oxide nanoparticles stabilized by alginate. Int J Pharm 2007;333:177-86.
41. Gao S, Shi Y, Zhang S, Jiang K, Yang S, Li Z, Takayama-Muromachi E. Biopolymer-Assisted Green Synthesis of Iron Oxide Nanoparticles and Their Magnetic Properties. J Phys Chem C 2008;112:10398-401.
42. Liu J, Zhang Y, Yang T, Zhang GS, Chen Z, Gu N. Synthesis, characterization, and application of composite alginate microspheres with magnetic and fluorescent functionalities. J Appl Polym Sci 2009;113:4042-51.
43. Chen K, Xie J, Xu H, Behera D, Michalski MH, Biswal S, Wang A, Chen X. Triblock copolymer coated iron oxide nanoparticle conjugate for tumor integrin targeting. Biomaterials 2009;30:6912-9.
44. Mu Q, Hondow NS, Krzemiński L, Brown AP, Jeuken LJ, Routledge MN. Mechanism of cellular uptake of genotoxic silica nanoparticles. Part Fibre Toxicol 2012;9:29.
45. He X, Nie H, Wang K, Tan W, Wu X, Zhang P. In vivo study of biodistribution and urinary excretion of surface-modified silica nanoparticles. Anal Chem 2008;80:9597-603.
46. South CR, Leung KC, Lanari D, Stoddart JF, Weck M. Noncovalent Side-Chain Functionalization of Terpolymers. Macromolecules 2006;39:3738-3744.
47. Chak CP, Xuan S, Mendes PM, Yu JC, Cheng CH, Leung KC. Discrete functional gold nanoparticles: hydrogen bond-assisted synthesis, magnetic purification, supramolecular dimer and trimer formation. ACS Nano 2009;3:2129-38.
48. Leung KC, Wang YX, Wang H, Xuan S, Chak CP, Cheng CH. Biological and magnetic contrast evaluation of shape-selective Mn-Fe nanowires. IEEE Trans Nanobioscience 2009;8:192-8.

Cite this article as: Leung KC, Sham KW, Chak CP, Lai JM, Lee SF, Wáng YX, Cheng CH. Evaluation of biocompatible alginate- and deferoxamine-coated ternary composites for magnetic resonance imaging and gene delivery into glioblastoma cells. Quant Imaging Med Surg 2015;5(3):382-391. doi: 10.3978/j.issn.2223-4292.2015.03.12

